Proceedings of the ASME 2022 Turbo Expo
Turbomachinery Technical Conference and Exposition
GT2022
June 13-17, 2022, Rotterdam, The Netherlands

GT2022-80226

IMPACT OF CENTRAL PILOTING ON THE STATIC AND DYNAMIC STABILITY OF SWIRL-STABILIZED FLAMES

Daniel Doleiden[1], Ashwini Karmarkar[1], Jacqueline O'Connor[1], James Blust[2]

[1]Mechanical Engineering, Pennsylvania State University, University Park, PA USA
[2]Solar Turbines Incorporated, San Diego, CA USA

ABSTRACT

One of the key challenges of lean, low-emissions combustor operation is flame stabilization, including both static and dynamic stabilization. Static flame stability encompasses a range of issues like flame holding, flashback, and blow-off. Dynamic flame stability refers to thermoacoustic combustion oscillations, which are driven by a coupling between combustor acoustics and flame heat release rate oscillations. Pilot flames are used as a passive means of achieving both static and dynamic stability in a number of gas turbine combustor technologies, likely by acting as a source of heat and radical species at the base of the main flame. Previous work used high-speed CH* chemiluminescence imaging to characterize the effect of a central pilot flame on the macrostructure and dynamic stability of a swirled lean-premixed natural gas-air main flame. In this study, the static and dynamic stability of the main flame are controlled by modifying the equivalence ratios of the main and pilot flames to better understand the mechanisms by which pilot flames enhance both static and dynamic stability. High-speed OH planar laser-induced fluorescence (OH-PLIF) is used to capture local instantaneous dynamics of the main and pilot flames across a range of operating conditions and stability outcomes, building upon the line-of-sight chemiluminescence analysis of the previous work. We find that the presence of the pilot flame controls anchoring of a relatively lean main flame. When the pilot flame is added to an unpiloted main flame, the main flame can rapidly change stabilization location, anchoring to the centerbody of the fuel injector. When a piloted main flame has the pilot removed, the flame lingers on the centerbody for a longer duration, likely due to the high-temperature boundary condition at the centerbody anchoring point. Further, the pilot flame mitigates combustion instability for a relatively broad range of operating conditions. Analysis of high-speed OH-PLIF shows that the main and pilot flames do not directly interact, and therefore the stabilizing mechanism of the pilot flame is indirect, as previously suggested.

Keywords: swirl flame, piloting, static stability, dynamic stability

NOMENCLATURE

DLN	Dry low NO_x
FOV	Field of view
L'	Lateral flame displacement fluctuation
P_{mean}	Mean pressure
P'_{RMS}	Pressure fluctuation level
PLIF	Planar laser-induced fluorescence
RMS	Root mean squared
T	Temperature
f_{inst}	Instability frequency
r	Radial coordinate
t	Time
x	Axial coordinate
Π	Pilot fuel percentage
ϕ	Global equivalence ratio

INTRODUCTION

Modern gas turbine engines obey strict criteria pollutant regulations through the use of lean combustion [1], which suppresses the formation of nitric oxides by reducing the temperature of the flame. Dry low-NO_x (DLN) combustor technology is implemented in a large number of power generation gas turbines [2–5] and increasingly used in aircraft engine combustors [6]. While these technologies have successfully reduced engine-out NO_x, other combustor operability challenges – namely static and dynamic stability issues – can arise from this combustion mode.

Static stability refers to the ability of the flame to achieve flame holding over a range of operating conditions. For example, in many power-generation and industrial gas turbine engines, DLN fuel injectors are designed to stabilize a flame at the end of a centerbody [7]; this is the configuration used in the current study. In this design, recirculation behind the centerbody in combination with vortex breakdown from the swirling flow enhance flame stabilization by creating a large central recirculation zone with shear layers on either side in which the flame can stabilize [8,9]. Static stability is lost when the flame

lifts from the centerbody, resulting in a weakly stabilized lifted flame, which can lead to flame blowoff.

Flame blowoff has been characterized in swirl-stabilized flames in a number of studies [10–12]. While the action of the central recirculation zone in swirling flames helps extend the blowoff limits as compared to non-swirling flames, blowoff is still possible at lean conditions used during low-emissions operation. During the blowoff process, flame extinctions occur along the flame edge, particularly at stabilization points, resulting in local weakening of the reaction and potential for reactant pockets to penetrate into the products zone. Spontaneous re-ignition in this region is possible, although closer to blowoff, the frequency of re-ignition decreases and the regions of extinction grow until the entire flame extinguishes.

Lean flames can also suffer from issues related to dynamic stability, which manifests as thermoacoustic instability driven by a coupling between combustor acoustics and flame heat release rate oscillations. In these cases, the lean flame is highly susceptible to incident perturbations, which can be excited by the incoming flow. Fluctuations in the flame heat release rate cause expansion in the flow around the flame, which when located near a pressure anti-node of the acoustic mode of the combustor, can couple in a feedback loop that leads to a high-amplitude, tonal instability. The instability amplitude is reached when the amplitude of thermoacoustic driving equals the damping in the system, at a point know as a limit cycle [13].

The thermoacoustic feedback loop is facilitated by one or more coupling mechanisms, which are physical processes inside the combustor, excited by the acoustic fluctuations, that drive further heat release rate oscillations [14]. In gas turbine systems, the most common coupling mechanisms are velocity coupling and mixture coupling. Velocity coupling arises when the acoustic mode excites velocity disturbances in the flow, particularly through shear layer excitation, that then cause large-scale flame area fluctuations as the flame wraps around the vortices shed in the shear layers [15,16]. These flame area fluctuations drive heat release rate fluctuations, which drive further acoustic oscillations to close the cycle. Mixture coupling arises when the acoustic pressure fluctuations drive fluctuations in fuel flow rate into the system [17,18], resulting in heat release rate fluctuations through a number of different pathways.

Pilot flames, or small flames in the region of a main flame, can help alleviate both static and dynamic flame stability issues. Some pilot flames operate in a diffusion mode, where fuel is directly injected into the region of the flame [19–22], and are sometimes used for active control. Other configurations use premixed or partially-premixed pilot flames [23–25]. Pilot flames may statically stabilize a main flame by acting as a passive source of heat and radical chemical species, promoting anchoring. A statically stable but dynamically unstable main flame may be dynamically stabilized by this same passive mechanism. Previous work from our group has suggested a mechanism by which piloting can suppress combustion oscillations and help increase static stability margins [25]. Here, it was observed that the stabilizing efficacy of a pilot flame depended strongly on pilot equivalence ratio but not pilot flow rate. Additionally, it was shown increasing pilot flame equivalence ratio increases efficacy until pilot flame equivalence ratio matches that of the main flame. These observations led to the hypothesis that piloting stabilizes the main flame by providing hot gases to the vortex breakdown region; these hot gases recirculate and enhance the static and dynamic stability of the main flame. It should be noted that piloting may also detrimentally affect the stability of the main flame. Previous work done on the apparatus in this study [26] showed piloting can statically stabilize a lifted flame, resulting in dynamic instability brought on by interaction of the anchored flame with vortices shed from the injector center body. The pilot flame itself may also become unstable, as seen in the computational and experimental work of Fu et al. [27].

The goal of the current study is to examine the impact of piloting on both the static and dynamic stability of a swirl-stabilized flame near the edge of its operability limits in a single-injector, optically-accessible combustor. This experimental configuration has been well-documented [25,26,28–30] and is one of the only facilities with a significant literature published on central premixed pilot flames. While we focus on a few particular operating conditions in this study, recent results by Li et al. [25] from both experimental and computational studies of this same configuration showed that the mechanism of piloting is similar over a wide operating range. Given these previous results and the relatively common injector configuration, we expect that the lessons learned from this study can be applied in other configurations and at other operating conditions. However, our previous studies have had limited diagnostic capability and have not considered the dynamics of the flame near blowoff. This study seeks to augment the dataset on this representative configuration by using high-speed OH-PLIF to explore the impact of central piloting on both static and dynamic stability.

In the first part of the study, we consider how piloting impacts static stability by observing the anchoring and blowoff processes of a flame when pilot is added and removed, respectively. Using high-speed planar laser-induced fluorescence of OH (OH-PLIF), we show how the pilot flame is the key to flame stabilization in this system and that flame anchoring is not significantly helped by the presence of recirculation in the corner of the combustor. In the second part of the study, we observe the impact that piloting has on the dynamic stability of the flame using the same OH-PLIF diagnostic. We conclude with discussions on how piloting can be effectively used to help enhance stability of flames in next-generation, low-emissions combustor designs.

EXPERIMENTAL METHODS

Experimental facility

Experiments are carried out in a swirled lean-premixed natural gas combustor. As shown in Figure 1, the combustor consists of an inlet section, an optically-accessible quartz liner, and a variable-length metallic section. The flame configuration includes a swirl-stabilized main flame and an axial jet pilot flame. The main flame is partially-premixed, where natural gas fuel is injected into the fuel injector through fuel injection holes

on the swirler vanes. The air flow rate in these experiments is held constant, while the main mixture equivalence ratio is controlled by varying the main fuel flow rate.

The pilot flame is fully-premixed and its equivalence ratio is controlled by varying the fuel flow rate to the pilot with a constant pilot air flow rate. The equivalence ratios of the pilot and main circuits are varied to keep the global equivalence ratio of the system constant, with pilot fuel flow rate (*Π)* ranging from 0-10% of the total fuel flow rate and pilot air flow rate fixed at 5.5% of the total air flow rate. Compressed air is metered through a Sierra 570S thermal-mass flow meter before being electrically preheated (T_{in} = 250 °C). Fuel for the main flame is metered through a Teledyne Hastings HFM-301 flowmeter, while fuel for the pilot flame is metered through a Teledyne Hastings HFM-D-301A flowmeter.

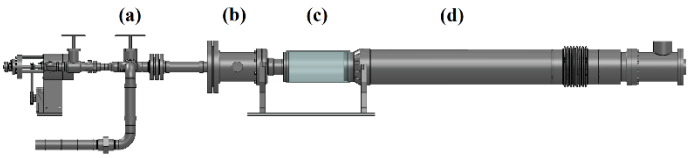

Figure 1: The experimental apparatus showing: a) the inlet section; b) the plenum; c) the quartz combustor; and d) the metallic variable-length combustor.

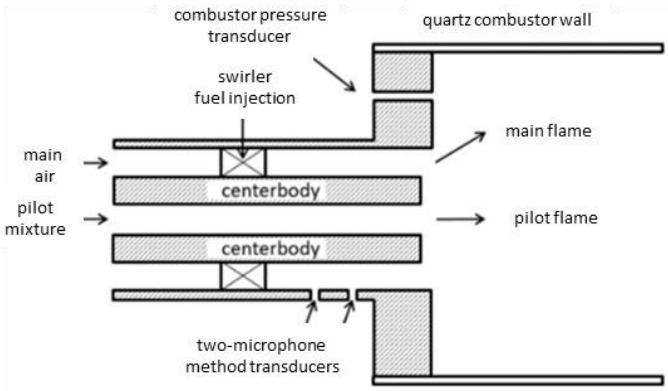

Figure 2: Schematic of the fuel injector showing the flow paths of the pilot mixture, the swirled main mixture, and the locations of the main and pilot flames inside the quartz combustor wall.

Figure 2 shows the structure of the injector, which is located downstream of the plenum and upstream of the quartz combustor section. Here, the main air flows through an annular passage containing an axial swirler before being injected into the quartz combustion chamber at the dump plane. The swirler blades in the injector have a trailing edge angle of approximately 45°. The pilot reactant premixture is fed through a central passage and injected along the central axis of the main flame without swirl. Reactant flow rates for the operating conditions considered in this study result in a bulk velocity of 40 m/s in the injector. The quartz combustor liner has a 15 cm diameter and 30.5 cm length, and allows the entire structure of the main and pilot flames to be accessed optically. The quartz combustor liner is coupled to a 12.3 cm inner diameter variable-length metallic section containing a water-cooled plug. A stepper motor-controlled traverser system (Isel-Automation) allows the overall combustor length between the dump plane and the water-cooled plug to be varied between 63.5-149.9 cm in increments of 0.25 cm, although all the analysis described in this paper was done at a combustor length of 63.5 cm. The ranges of operating parameters relevant to this study are tabulated in Table 1.

Table 1: Operating conditions

Global equivalence ratio (ϕ)	0.52, 0.55, 0.58, 0.60, 0.62, 0.64, 0.65
Combustor length (L_{comb})	63.5 cm
Pilot fuel flowrate as percent of total fuel flowrate *(Π)*	0, 3%, 6.5%, 8%, 10%
Pilot air percentage	5.5%
Air inlet temperature (T_{in})	250 °C

Diagnostics

Water-cooled dynamic pressure transducers (PCB) are mounted in recesses in the dump plane, the air passage of the fuel injector, and the main fuel system. The global chemiluminescence is measured using a photomultiplier tube fitted with a 432 nm narrow band-pass filter. Pressure and global chemiluminescence are sampled simultaneously at a rate of 8132 Hz. The dynamic structure of the flame is evaluated via CH* chemiluminescence images captured with a Photron Fastcam SA4 camera coupled to an Invisible Vision UVi intensifier. This combination allows images of the entire structure of the main and pilot flames to be captured with a frame rate of 4000 frames per second, an exposure time of 200 μs, and a resolution of 79 pixels per inch. For each operating condition, 8 seconds of pressure and global chemiluminescence data are taken, and one second (4000 frames) of high-speed images are taken.

Planar laser-induced fluorescence of OH is used to visualize ground-state hydroxyl radicals within a laser sheet, allowing flame edges to be defined with high spatial and temporal fidelity. A pump laser (Edgewave Innoslab IS200-2L Nd:YAG diode laser) is used with a rhodamine chloride dye laser (Sirah Credo high-speed dye laser) to produce an approximately 1.2 W beam. The beam is pulsed at 10 kHz with a wavelength of 282.9 nm. Images are taken at 10 kHz using a high-speed camera (Photron SA 1.1) equipped with an intensified relay optic (LaVision HS-IRO) and an ultra-violet lens (Cerco 100mm f/2.8). A 320 nm filter (LaVision 1108760 VZ-Image) isolates OH fluorescence emission. 10,000 images are captured at each operating condition. An optical chain consisting of ultra-violet mirrors, positive and negative cylindrical quartz lenses, and a periscope is used to steer and collimate the laser beam into a vertical sheet approximately 40 mm high. In this paper, we discuss results measured in several 20 mm sheets located near the dump plane to capture the dynamics of the flame near its attachment point and in the region where the flame impinges on the quartz liner.

Data Analysis

The stability of the combustor is characterized quantitatively by determining the root-mean-squared (RMS) level of the acoustic pressure fluctuation at the dump plane (P'_{RMS}) within a ±10 Hz band centered about the instability frequency for each operating condition. The combustor is considered to be unstable when the normalized pressure RMS level (P'_{RMS}/P_{mean}) exceeds 0.01. High-speed CH* chemiluminescence imaging produces line-of-sight integrated projection images. Spatial high-frequency noise is reduced via background subtraction and median filtering. A time-averaged emission image representing heat release intensity on a 2-D plane is obtained by application of a Hankel-Fourier operator to perform an inverse Abel transform. Profiles representative of CH* emission integrated over the azimuthal coordinate are obtained by a radial weighting factor of $2\pi r$.

High-speed OH planar laser induced fluorescence images show regions of OH in high spatial and temporal fidelity. Power distribution within the laser sheet was visualized with acetone vapor fluorescence. A sheet correction profile was then generated to reduce uncertainty associated with uneven power distribution. Sheet corrected images were either analyzed as-is or binarized for qualitative analysis. Binarization marks each pixel in an image as either a region of products (value of 1) or a region of reactants (value of 0). Before binarization, a bilateral filter and a Gaussian blur were used to reduce noise. Gradients in the images were found with the Prewitt method, and the Sobel method was used for multi-level thresholding. The resulting binarized image is sensitive to some of the parameters chosen for each of these processing steps. A detailed discussion of these sensitivities in the context of turbulent flames and this particular imaging setup is discussed in the supplementary material of Tyagi et al. [31].

Binarized image sets were time-averaged to produce time-averaged progress variable fields. These fields represent the likelihood of flame presence at a given location on a scale from 0 (reactants) to 1 (products). An edge tracking algorithm was applied to binarized images to locate the main flame edge in space and time; identifying the location of the pilot flame was not possible due to relatively weak intensity gradients in the pilot region of each field of view. Care was taken during edge extraction to ensure that the calculated edges aligned with the visible edge in the original images; the authors visually inspected each of the datasets to ensure a good match. The edge tracking algorithm yields a timeseries of flame edge oscillation (L') at each downstream distance. Previous work by Shanbhogue et al. [32] showed using both theory and experiment that the lateral displacement of the flame in a velocity-coupled instability was a useful marker for flame area oscillations, and hence heat release rate oscillations. Flame edge oscillation was quantified by performing a Fast Fourier Transform on the L' timeseries. This analysis provides waterfall plots of single-sided power spectral density at each downstream distance within the first field of view; analysis of subsequent fields of view was not possible due to frequent flame impingement on the combustor liner and relatively low intensity gradients that made edge detection unreliable.

RESULTS AND DISCUSSION

Flame stability and structure

The static and dynamic stability of the main flame are assessed by quantifying dynamic pressure fluctuation RMS (P'_{RMS}) and by examining high-speed CH* chemiluminescence image sets. At the operating conditions and combustor length considered in this study, we observe a self-excited instability mode termed Mode I (f_{inst} = 168 Hz). Figure 3 shows a dynamic stability map at this combustor length as a function of the global equivalence ratio, ϕ, and the piloting level, Π. The color on this map indicates the pressure fluctuation amplitude at the instability frequency normalized by the mean combustor pressure. The map also shows the regions where the flame is attached to the centerbody and where it is not; the region at low equivalence ratios bounded by the dotted white line is the region where the flame is lifted and aerodynamically stabilized. The main flame is attached to the centerbody under most operating conditions considered, with flame lift at unpiloted global equivalence ratios leaner than ϕ = 0.55 and piloted global equivalence ratios below approximately ϕ = 0.525. Flame lift was verified by direct observation and by evaluation of time-averaged chemiluminescence images.

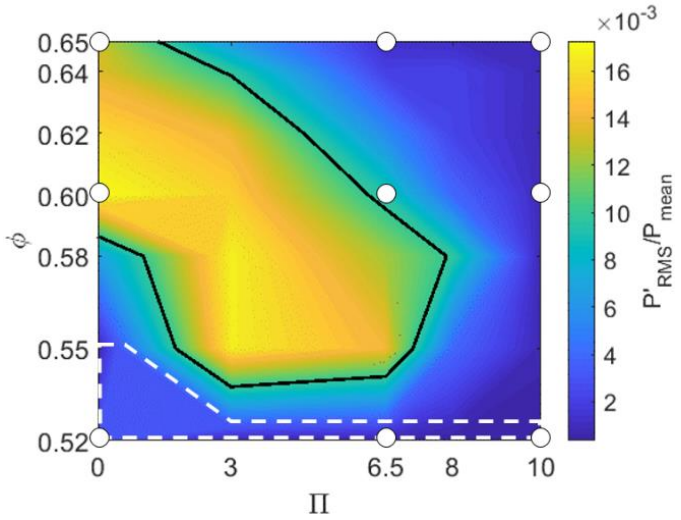

Figure 3: 2-D dynamic stability map showing dump plane pressure fluctuation RMS (P'_{RMS}) as a function of global equivalence ratio (ϕ) and pilot percentage (Π).

At the lowest global equivalence ratios ($\phi < 0.525$), piloting affects neither the static nor the dynamic stability of the main flame; the main flame remains lifted regardless of pilot percentage and the flame does not exhibit thermoacoustic oscillation. At low to intermediate equivalence ratios ($0.525 < \phi < 0.58$), the main flame is lifted without piloting. The diversion of a small amount of fuel through the pilot circuit anchors the main flame at these equivalence ratios, subjecting the base of the main flame to vortices shed from the injector centerbody and providing a coupling mechanism to drive the instability. Further fueling of the pilot flame reduces the amplitude of the instability, with full stabilization achieved with Π=6.5% or 8% piloting.

Intermediate to high global equivalence ratios ($\phi > 0.58$) produce a statically stable but dynamically unstable main flame without piloting. Less fuel diversion through the pilot flame is required to effectively suppress the instability at intermediate to high equivalence ratios than at low to intermediate equivalence ratios.

Single-sided power spectral densities of dump plane dynamic pressure fluctuation at selected global equivalence ratios are provided in Figure 4; their locations on the stability map are shown in white circles in Figure 3. At $\phi = 0.52$, some coherence is observed at the frequency associated with Mode I, although it does not meet the criterion for unstable in this combustion system. At $\phi = 0.60$, a well-defined peak in pressure oscillation is present at the frequency of Mode I and several of its harmonics, an indication of nonlinear behavior due to the high-amplitude limit cycle oscillations. Addition of the pilot flame reduces the power in this portion of the spectrum but low-amplitude coherent oscillation is maintained even with heavy piloting. Several harmonic peaks are visible at each pilot percentage. At $\phi = 0.65$, coherent oscillations of relatively high amplitude and several harmonic peaks are observed when the pilot flame is absent. The addition of the pilot flame effectively eliminates coherent oscillations.

The structure of the unpiloted and piloted main flames at selected operating conditions (ϕ = 0.52, 0.60, 0.65; Π = 0%, 6.5%, 10%) are characterized by examining time-averaged CH* chemiluminescence images (Figure 5). Here, the $\phi = 0.52$ main flame is visibly lifted without piloting; the base of the flame aerodynamically stabilizes approximately 5 cm downstream of the dump plane. Heat release primarily occurs in the corner recirculation zone. Moderate piloting (Π = 6.5%) causes the main flame to anchor by propagating towards the fuel injector center body, and heat release shifts primarily to the inner shear layer with a reduction in intensity evident in the corner recirculation zone. Heavy piloting ($\Pi = 10\%$) elongates the main flame as a considerable percentage of fuel is diverted away from the main flame, thus lowering its equivalence ratio and decreasing its flame speed.

The $\phi = 0.6$ main flame is visibly attached to the fuel injector centerbody without piloting, and heat release occurs mostly in the inner shear layer. The significant area over which heat release is present in this case is a result of the large-scale motions from the thermoacoustic instability. Moderate piloting (Π = 6.5%) thins the profile of the main flame as dynamic stabilization occurs, and also causes heat release to shift into the corner recirculation zone. Heavy piloting ($\Pi = 10\%$) fully dynamically stabilizes the main flame, with heat release concentrated in a relatively thin band along the inner shear layer. The time-averaged structure of the unpiloted $\phi = 0.65$ main flame exhibits a relatively compact structure compared to the ϕ = 0.60 main flame, due to both the increase in flame speed of the main mixture and the relatively lower oscillation amplitude, where oscillations increase the thickness of the flame brush in these time-averaged images. Piloting stabilizes the main flame at ϕ = 0.65 in a similar fashion to $\phi = 0.60$, though penetration in the corner recirculation zone is much less pronounced at $\phi = 0.65$.

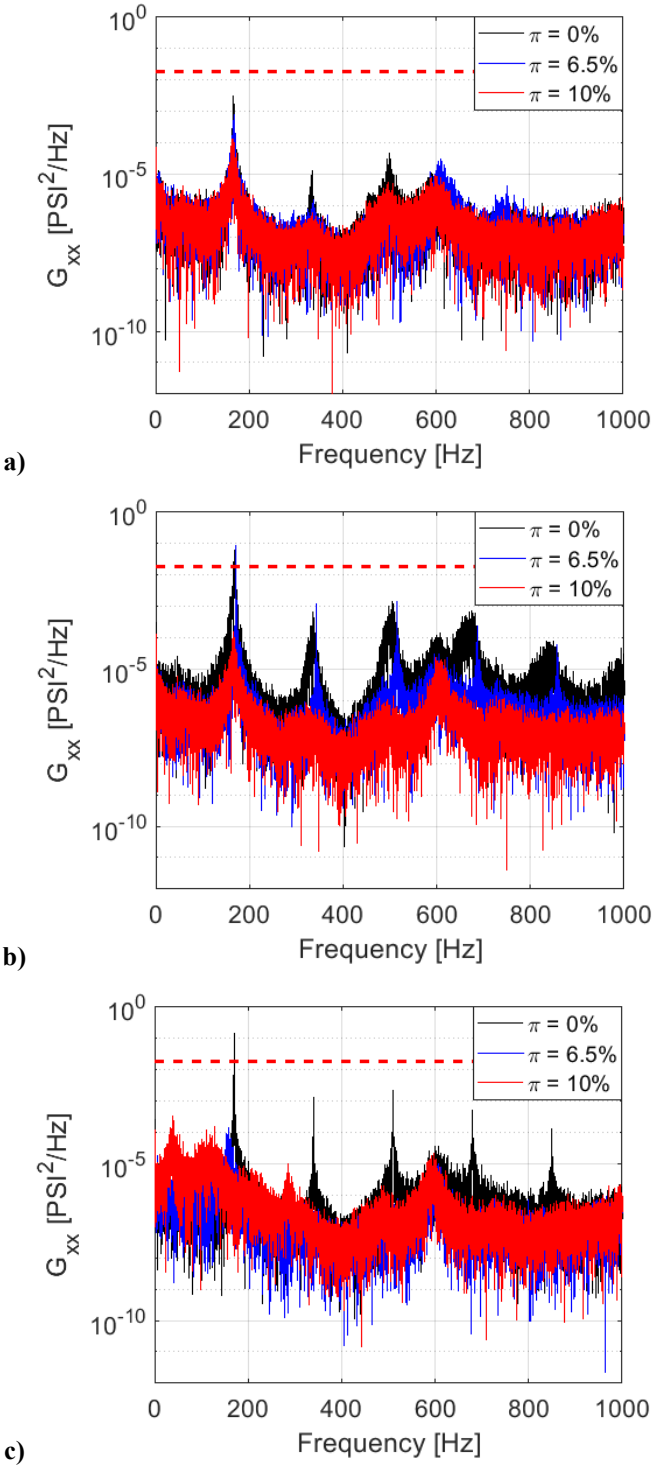

Figure 4: Single-sided power spectral density of dump plane dynamic pressure fluctuation (P'_{RMS}) at a) ϕ=0.52, b) ϕ=0.60, and c) ϕ=0.65.

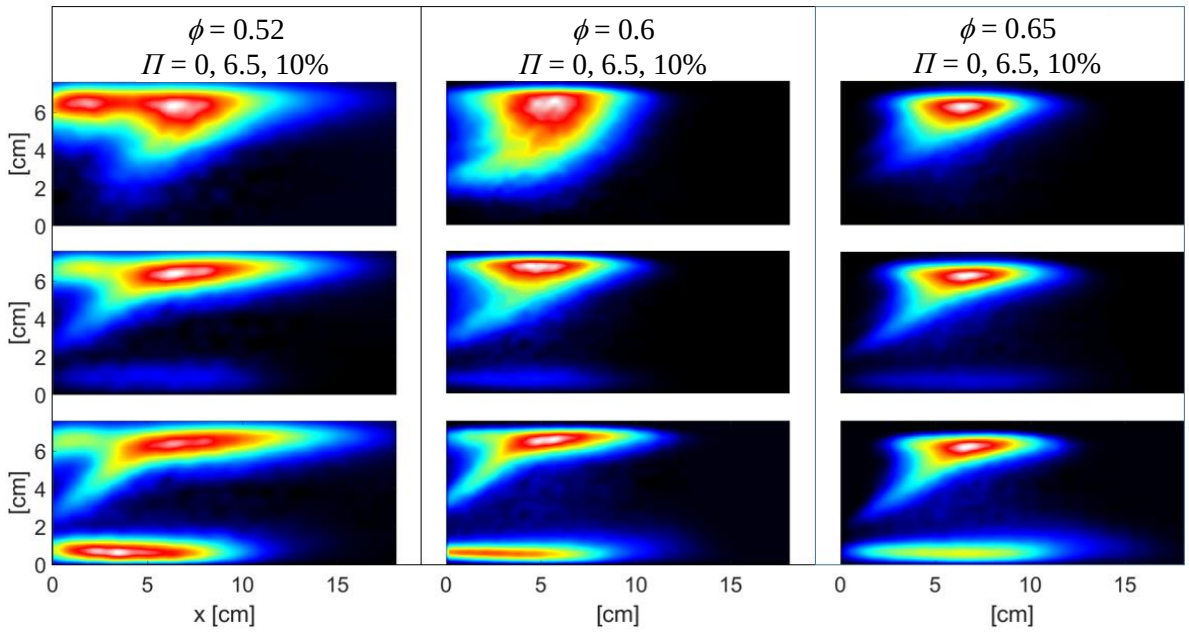

Figure 5. Time-averaged chemiluminescence imaging of the piloted flame at three equivalence ratios.

Impact of piloting on static stability

To understand the impact of the pilot on static stability and flame anchoring, we analyze transient OH-PLIF imaging to observe flame attachment (with the addition of pilot) and liftoff (with the removal of pilot). In these transient cases, the global equivalence ratio changes as the pilot flame is turned on and off in order to see the changes that only the pilot has on the flame, rather than a combination of the pilot and the main equivalence ratio. As such, the main flame equivalence ratio is held constant throughout both tests.

Transient attachment

The operational procedure for transient attachment testing is as follows. First, we begin with the main and pilot flames on at ϕ = 0.52 and Π = 10% and wait for the flame to stabilize and the system to thermally equilibrate to the baseline condition; previous experimental experience of transient testing in this research group has shown the importance of establishing a baseline thermal condition before a transient test is run [33]. Next, we turn the pilot off and wait until the main flame lifts from the centerbody and is aerodynamically stabilized. At that point, without much delay, we record OH-PLIF images and turn the pilot flame back on to Π = 10%, increasing the global equivalence ratio to ϕ = 0.52. This transient is shown in Figure 6, which provides a filmstrip view of a sequence of snapshots that illustrate the re-attachment process. At t = 111 ms, the flame is lifted out of the field of view, and hence no signal is observed.

Figure 6 shows that as the pilot is turned on, at around t = 115 ms, the main flame begins to re-attach. Eventually, at t = 120 ms, hot products are recirculated into the corner recirculation zone and the flame reaches its final state. To understand the transient behavior of the pilot flame, the main flame, and the corner recirculation zone, we record the PLIF signal intensity at three probe locations-in the pilot flame, the main flame, and in the corner recirculation zone, as shown by the three probe locations in Figure 6. The probe consists of OH-LIF signal averaged over a 3 × 3 pixel window to avoid spurious results from single point measurements. Note that the laser sheet propagates across the field of view from left to right, which is the reason why the left-hand side of the image is brighter than the right-hand side of the image.

Figure 7a and Figure 7b show the probe measurements for all three probe locations for two repeated tests run at the same conditions. The purpose of this analysis is to visualize the shape of the time history of the OH-PLIF intensity in these regions; the actual intensity numbers do not have any meaning as this is not a quantitative LIF technique. In the first run, corresponding to the filmstrip in Figure 6, the main flame appears nearly as soon as the pilot flame is ignited at t=115 ms. As we are unable to visualize the fuel injection process, it's unclear how fuel from the pilot is transported before it ignites, but the pilot ignition and main flame attachment process happen rapidly together. In both the pilot and the main flame, there is an initial burst of intensity and then the OH intensity stabilizes; this initial burst of heat release at ignition has previously been seen in the ignition of gas turbine combustors [34]. OH intensity in the corner recirculation zone appears soon after the pilot and main flames, but its presence is intermittent. Figure 7b shows the probe measurements for the second repeat run at the same conditions. In this run, the recirculation zone is always present, possibly due to remaining products from the first run. Like in the first run, as the pilot flame ignites, the main flame appears with it, and after an initial burst of intensity, the main flame and pilot flame intensities stabilize.

The two runs illustrate the importance of the pilot in stabilizing the main flame and ensuring the flame is anchored at

the centerbody. Introducing the pilot flame can cause a lifted flame to attach to the centerbody. The probe plots show that the presence of the corner recirculation zone does not have much impact on the process of main-flame anchoring, as similar processes occur in both film strips (second test not shown for brevity) and in both probe time series. While the time-averaged chemiluminescence imaging in Figure 5 shows significant presence of the flame in the corner recirculation zone at statically stable conditions, the corner recirculation zone does not play a dynamical role in stabilizing the flame during attachment.

Transient Lift-off

Like in the transient attachment tests, we begin the transient lift-off tests with the main and pilot flames on at $\phi = 0.52$ and $\Pi = 10\%$ and wait for the flame to stabilize and the system to thermally equilibrate to the baseline condition. We then begin recording OH-PLIF images and turn the pilot fuel off. Figure 8 shows a filmstrip view of a sequence of snapshots to illustrate the flame dynamics as the pilot is turned off.

The snapshots are 10 ms apart since the detachment process is slower than the attachment process shown in Figure 6. Previous studies have shown how gradual and intermittent flame blowoff can be, particularly in bluff-body stabilized flames where the recirculation of hot products can act as an ignition source after local extinction of the flame [35,36]. As the pilot fuel is cut at around $t = 150$ ms, the main flame becomes weaker but remains attached. The corner recirculation zone is present as well and is not significantly impacted by the loss of the pilot flame. Like in the transient attachment condition, we observe the LIF signal intensity at three probe locations-in the pilot flame, the main flame and in the recirculation zone. The probe locations are shown using markers in Figure 8. The signal is averaged over 3×3 pixel window, to avoid spurious results from single point measurements.

Figure 9a shows the probe measurements for all three probe locations for two repeated tests run at the same conditions. In the first run (corresponds to the filmstrip), the signal of the main flame weakens as the pilot fuel flow is turned off at $t = 150$ ms, but the main flame is still present despite the lack of pilot flame. The corner recirculation zone is present throughout and is not impacted by the absence of the pilot. Figure 9b shows the probe measurements for the second run at the same conditions. Again, the main flame weakens as the pilot fuel flow is cut, but the flame does not extinguish. The recirculation zone, in this case, disappears eventually, but the main flame remains for the duration of the OH-PLIF data acquisition. Observation of the flame after the OH-PLIF acquisition showed that the main flame does eventually lift and return to the aerodynamically stabilized location that is seen in the beginning of the flame attachment film strip of Figure 6. However, this process takes on the order of seconds, rather than the milliseconds that flame attachment takes, and the image storage capacity on the camera is not high enough to capture events that take several seconds.

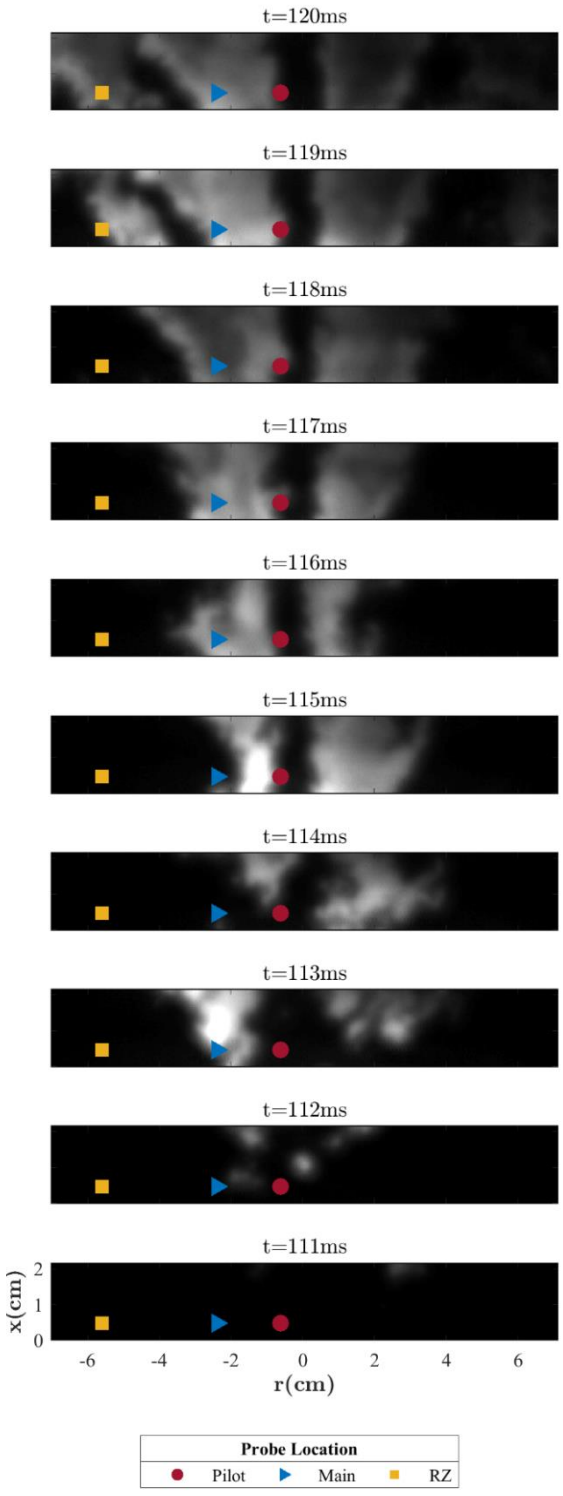

Figure 6: Sequence of snapshots illustrating the attachment of the main flame when pilot fuel is added; field of view shows the very base of the flame.

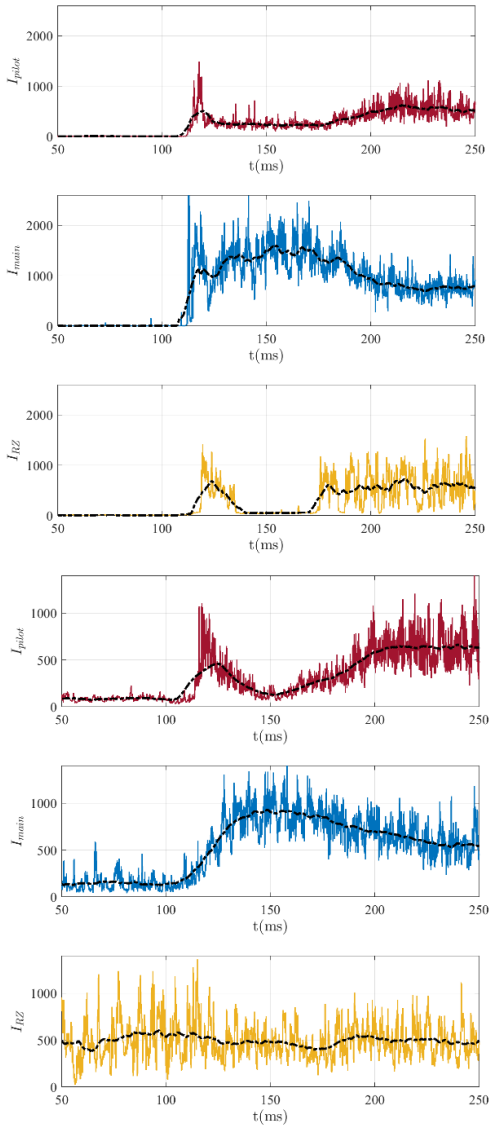

Figure 7. Time series of OH-PLIF probes from Figure 6 for two experimental repeats of the flame attachment process (a, b).

Put together, the two runs indicate that while removing the pilot fuel flow does reduce the signal intensity of the main flame close to the centerbody, the main flame remains anchored for the duration of the record and long afterwards. Compared to the transient attachment condition, the timescales for lift-off are significantly longer. This is likely due to the fact that the hot products present in the central recirculation zone on the products-side of the flame help keep the main flame anchored for longer once the pilot is turned off. This hysteresis in the response of the flame to the presence of the pilot flame is a key observation that can help better understand the limits of operability of the combustor. The transient measurements together show that the pilot flame controls the attachment process, but that once a central recirculation zone is established, it back-supports the flame and can extend the blowoff limits.

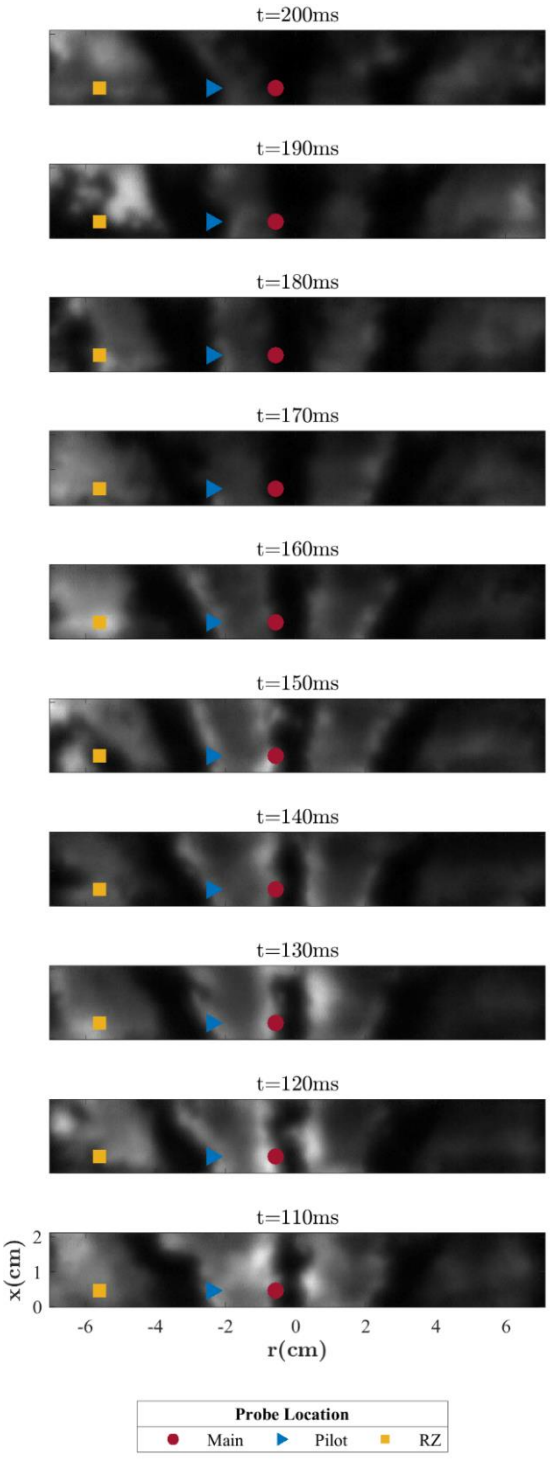

Figure 8: Sequence of snapshots illustrating the transient blow-off process as pilot fuel is removed; field of view shows the very base of the flame.

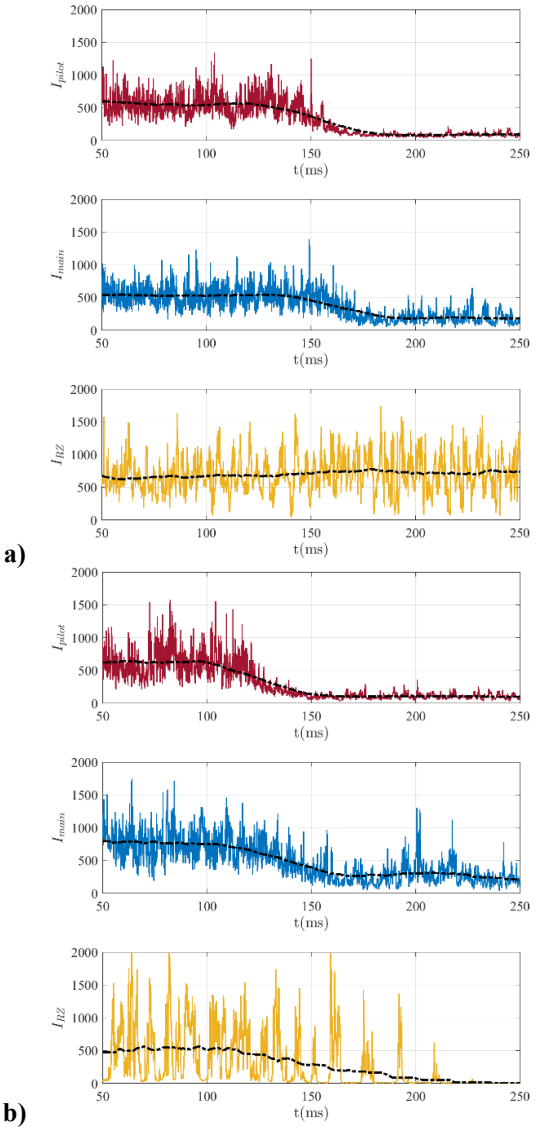

Figure 9. Time series of OH-PLIF probes from Figure 8 for two experimental repeats of the flame blow-off process (a, b).

Work by Coriton et al. [37], Zhang et al. [38], Foley et al. [39], and Shanbhogue et al. [9] have shown the critical role that product back-support plays in stabilizing flames in regions of high shear. Once the back-support from recirculating products in the central recirculation zone has been established, it can support the flame and extend the lean extinction limit that would normally be seen in a flame without back-support. Recent simulations of this facility confirmed the importance of back support on flame stabilization [25]. A high-fidelity large-eddy simulation of this flame at $\phi_{main} = 0.6$ and varying pilot fuel and air flow rates showed that a pilot flame with a lower equivalence ratio than the main flame can weaken the flame near its attachment point by lowering the temperature and radical concentration in that region. Pilot flames with equivalence ratios higher than that of the main flame enhanced the temperature and radical concentration, thereby enhancing the reaction rates in the flame anchoring region. While the pilot flame is an extra source of back support that can dramatically extend the local lean extinction limits at the attachment point of the flame, even the action of product recirculation has enough effect to cause the flame to linger after the pilot flame is gone.

Impact of piloting on dynamic stability

To understand the influence of the pilot flame on dynamic stability, the dynamics and interaction of the pilot and main flames were characterized using OH-PLIF imaging at steady conditions, rather than the transient conditions of the previous section. First, time-averaged progress variable contours were calculated by binarizing OH-PLIF image sets of the $\phi = 0.60$ condition without piloting ($\Pi = 0\%$) and with piloting ($\Pi = 10\%$) across two fields of view; these are shown in Figure 10. The first field of view is adjacent to the dump plane and the second field of view is immediately downstream from the first field of view. Overlaid time-averaged progress variable contours denote boundaries of 20%, 50%, and 80% reaction progress. The unpiloted main flame is evident at $r = 3$ cm in the first field of view and $r = 4$ cm in the second field of view. The corner recirculation zone is seen in the top of both fields of view. The 20% progress contours show that the main flame and the corner recirculation zone do not directly interact in most of the first field of view, with some merging evident in the furthest downstream portion of the frame. This merging is pronounced in the second field of view, with the 50% progress contours beginning to merge as distance from the dump plane increases. The progress variable contours emanating from $r = 0.8$ cm of the unpiloted cases show a value of 0 along the centerline in the region of the pilot jet, but there is no fuel here in these cases, only air. As such, the progress variable cannot be interpreted in this region, as the images show the interface between air and products, not reactants and products.

In the unpiloted case, the main flame brush, or the distance between the 20% and 80% contours in the main flame, is quite large. This width is a result of not just turbulent flame wrinkling, but mostly a result of the large-scale flame wrinkling from the combustion instability. In this case, it is likely that vortices are shed from the shear layer separation point at the end of the centerbody, resulting in large-scale wrinkles on the flame, as will be shown in Figure 11. These coherent oscillations have a much larger effect on the flame brush than the turbulent wrinkling. Progress variable contours of the piloted main flame show the same regions as in the unpiloted flames, but now a much narrower flame brush. In this case, the thermoacoustic instability is suppressed and so the large-scale wrinkling is no longer present. Merging of the main flame and corner recirculation zone is not present in field of view (FOV) 1 because of the reduced coherent flame wrinkling, and only present at large downstream distances in field of view 2. A region of products is readily visible between the main and pilot flames in both fields of view. This region, along with the time-averaged flame structure obtained from CH* chemiluminescence, suggests that the pilot flame acts indirectly on the main flame, providing a passive source of heat

and radical chemical species as opposed to direct flame-flame interaction.

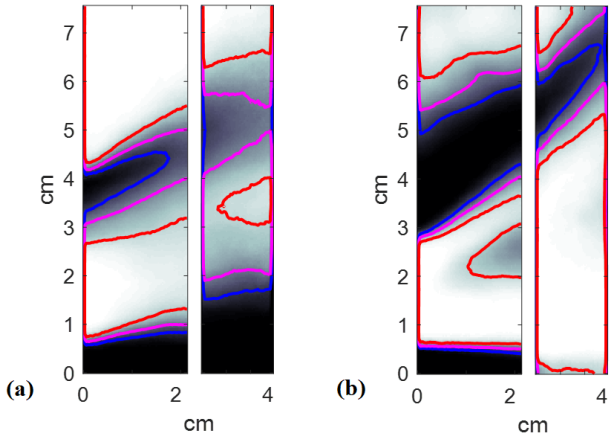

Figure 10: Time-averaged progress variable fields generated from binarized images of the (a) unpiloted (Π= 0%) and (b) piloted (Π= 10%) $\phi = 0.60$ main flames. Overlaid contours denote regions of 20% (blue), 50% (magenta), and 80% (red) reaction progress.

Film strip views of instantaneous OH-PLIF images of the unpiloted and piloted main flames are provided in Figure 11. In these images, flow goes from left to right, and data collection in the three downstream regions is *not* simultaneous; the time progression in each FOV is consistent one frame to the next, but each of the FOVs were obtained in different experimental runs. In these images, large-scale oscillations are observed in the unpiloted main flame, suggesting interaction with vortices shed from the dump plane; it should be noted that a simultaneous velocimetry study was not performed, but the mechanism of vortex shedding in velocity-coupled instability is well-established and matches the flame wrinkling patterns in the OH-PLIF. The addition of a pilot flame eliminates this coherent motion, suggesting decoupling of the instability feedback cycle. Direct flame-flame interaction between the main flame and the pilot flame is not observed in these images.

Previous work in this configuration in a study using chemiluminescence imaging and high-fidelity large-eddy simulation showed that the mechanism by which the pilot suppresses instability is through "back support" [25]. In this case, the heat and radical species generated by the pilot flame in the region of main-flame stabilization helps to improve the dynamic stability, as well as the static stability. One unanswered question from the chemiluminescence imaging, however, was whether the pilot and main flames ever directly intersected. This new PLIF imaging shows that there is no direct intersection between the main and pilot flame fronts, only thermochemical influence through the back support mechanism.

To quantify the effect of piloting on flame edge displacement, an edge tracking algorithm was used to capture flame edge position fluctuation (L') as a function of downstream distance and time. This algorithm locates flame edges in

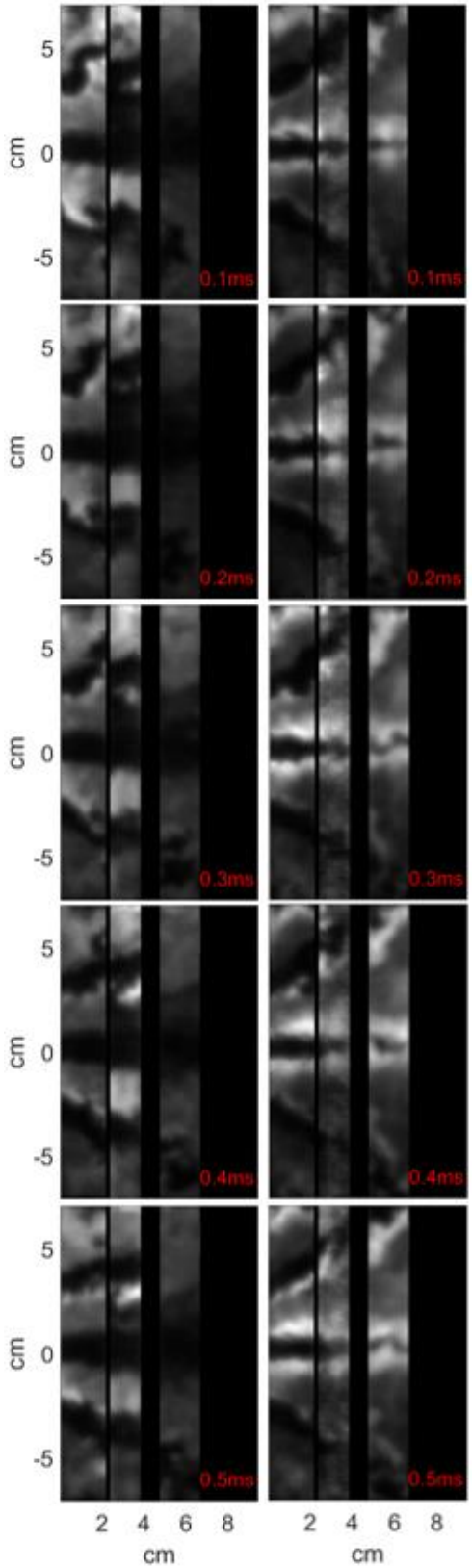

Figure 11: Filmstrip sequences of OH-PLIF images of the unpiloted (Π= 0%) and piloted (Π= 10%) φ = 0.60 main flames in three successive fields of view.

binarized image sets of the unpiloted and piloted main flame in the first field of view; analysis of downstream fields of view was not possible due to lower image intensity at these positions. The flame displacement time series is a measure of the extent of flame wrinkling, as described by Shanbhogue et al. [32]. Large-scale coherent flame wrinkling displaces the flame outward as the flame wraps around each passing vortex. By inspecting the frequency-domain characteristics of the flame displacement, we can quantify information about the local heat release rate oscillations in a velocity-coupled instability from the gain of the spectrum, and information about the wrinkle convection velocity from the phase of the spectrum.

The power spectral density (PSD) of L', G_{xx}, was calculated at each downstream distance in field of view 1 and is presented as a waterfall plot in Figure 12. Peaks in the PSD provide an indication of coherent activity in the displacement of the flame. In Figure 12a for the unpiloted case, coherent oscillation of the main flame edge is evident at all downstream distances, with the magnitude of the oscillation increasing with distance from the centerbody. Almost no oscillation occurs at frequencies other than the instability frequency and its harmonics. This result suggests that the motion of the main flame is dominated by coherent oscillations, most likely driven by vortices shed from the centerbody.

Addition of the pilot flame (Π= 10%), shown in Figure 12b, fully stabilizes the main flame, decoupling the instability feedback cycle and eliminating large-scale coherent edge oscillation. The spectrum in this case is very noisy, with no discernable monocomponent oscillation pattern. Additionally, the oscillations occur at greatly reduced amplitudes. The extent of flame displacement increases with downstream distance as the turbulence in the shear layer develops and wrinkles in the flame increase in size [40]. However, because there is no thermoacoustic feedback in this case, no coherent vortical fluctuations are generated in the shear layer and so no coherent wrinkles on the flame are formed.

CONCLUSIONS

This study focuses on understanding the impact of introducing a central pilot flame in a swirl stabilized combustor. The goal of this work is to visualize the individual mechanisms that govern the efficacy of the pilot in enhancing flame stabilization using high-speed planar laser-induced fluorescence of OH. We have chosen a combustor length in this variable-length combustor where the flame stabilization location and thermoacoustic instability are sensitive to both global equivalence ratio and percentage of fuel diverted to the pilot flame.

Using transient data at two conditions, we study the effect that introducing and removing fuel to the pilot flame can have on the static stability of the main flame. Our results show that, in the case of a lifted main flame with no pilot fuel, introducing the pilot flame causes the main flame to reattach rapidly and eventually reach stable attachment on the centerbody. Here, the presence of a corner recirculation zone alone is not sufficient for the main flame to reattach; the pilot must be introduced. In the second condition, we observe the response of an anchored flame to the pilot fuel being turned off. Here, the main flame weakens but does not immediately detach from the centerbody, instead lasting for several seconds before lifting to the aerodynamically stabilized position. In this case, too, the presence of the corner recirculation zone does not significantly affect the flame anchoring behaviors.

We also characterize the dynamic stability of the flame and the impact of central piloting on thermoacoustic oscillations by observing the flame edge oscillations of the main flame. Our results show that, in the absence of the pilot, the main flame is unstable and coherent flame displacement can be seen at the instability frequency. As the pilot is introduced, the single frequency tonal modes disappear; instability is suppressed.

Put together, these results illustrate the significance of the central pilot flame on both the static and dynamic stability of the main flame. In combustors with pilot flames, it is likely the controlling aspect of flame stabilization, where the corner recirculation zone has a significantly weaker influence. This work, put together with previous work on this piloted swirl-stabilized flame configuration provides interesting insight towards the design of pilot flames for both static and dynamic flame stabilization.

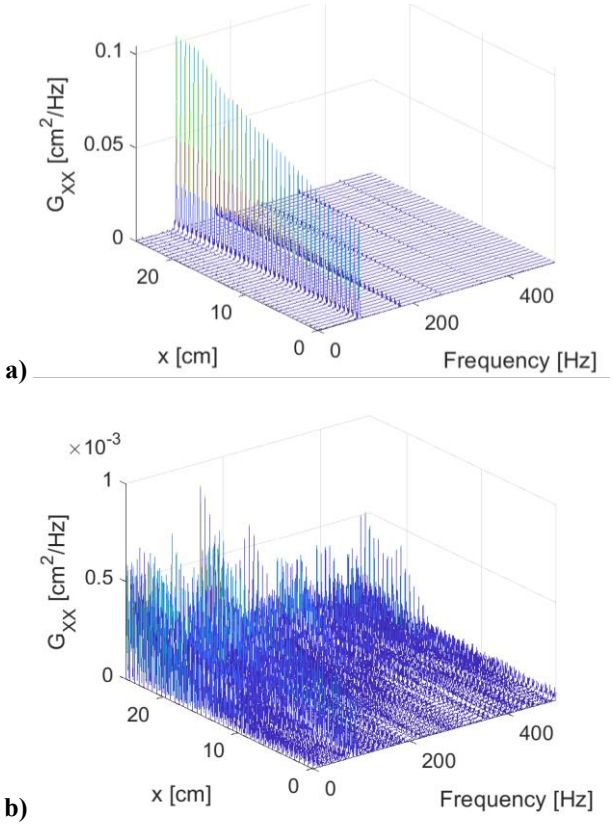

Figure 12: Single sided power spectral density of flame edge position fluctuation (L') for the a) unpiloted (Π = 0%) and b) piloted (Π = 10%) ϕ = 0.60 main flames.

ACKNOWLEDGEMENTS

The authors are grateful for the financial support from Solar Turbines Incorporated with program monitor Dave Voss.

REFERENCES

[1] Lieuwen, T. C., and Yang, V., 2013, *Gas Turbine Emissions*, Cambridge University Press, New York, NY.

[2] Steele, R. C., Cowell, L. H., Cannon, S. M., and Smith, C. E., 2000, "Passive Control of Combustion Instability in Lean Premixed Combustors," J. Eng. Gas Turbines Power, **122**(3), pp. 412–419.

[3] Davis, L. B., and Black, S. H., 1996, "Dry Low NOx Combustion System for GE Heavy-Duty Gas Turbines," *Proceedings of the ASME Turbo Expo*, Birmingham, UK.

[4] Diakunchak, I. S., Gaul, G. R., McQuiggan, G., and Southall, L. R., 2002, "Siemens Westinghouse Advanced Turbine Systems Program Final Summary," *Turbo Expo: Power for Land, Sea, and Air*, pp. 967–974.

[5] Tanimura, S., Nose, M., Ishizaka, K., Takiguchi, S., and Rodriguez, J., 2008, "Advanced Dry Low NOx Combustor for Mitsubishi G Class Gas Turbines," *Turbo Expo: Power for Land, Sea, and Air*, pp. 607–615.

[6] Foust, M., Thomsen, D., Stickles, R., Cooper, C., and Dodds, W., 2012, "Development of the GE Aviation Low Emissions TAPS Combustor for next Generation Aircraft Engines," *50th AIAA Aerospace Sciences Meeting Including the New Horizons Forum and Aerospace Exposition*, p. 936.

[7] Smith, K. O., Rawlins, D. C., and Steele, R. C., 2000, "Developments in Dry Low Emissions Systems," *International Pipeline Conference*, American Society of Mechanical Engineers.

[8] Chterev, I., Foley, C. W., Foti, D., Kostka, S., Caswell, A. W., Jiang, N., Lynch, A., Noble, D. R., Menon, S., and Seitzman, J. M., 2014, "Flame and Flow Topologies in an Annular Swirling Flow," Combust. Sci. Technol., **186**(8), pp. 1041–1074.

[9] Shanbhogue, S. J., Sanusi, Y. S., Taamallah, S., Habib, M. A., Mokheimer, E. M. A., and Ghoniem, A. F., 2016, "Flame Macrostructures, Combustion Instability and Extinction Strain Scaling in Swirl-Stabilized Premixed CH4/H2 Combustion," Combust. Flame, **163**, pp. 494–507.

[10] Cavaliere, D. E., Kariuki, J., and Mastorakos, E., 2013, "A Comparison of the Blow-off Behaviour of Swirl-Stabilized Premixed, Non-Premixed and Spray Flames," Flow, Turbul. Combust., **91**(2), pp. 347–372.

[11] Kumar, R. M., Chterev, I., Stepien, D., Sirignano, M., Emerson, B. L., Fugger, C. A., Jiang, N., Roy, S., and Lieuwen, T. C., 2021, "Near Blowout Dynamics of a Premixed, Swirl Stabilized Flame," Proc. Combust. Inst., **38**(4), pp. 6067–6075.

[12] Stöhr, M., Boxx, I., Carter, C., and Meier, W., 2011, "Dynamics of Lean Blowout of a Swirl-Stabilized Flame in a Gas Turbine Model Combustor," Proc. Combust. Inst., **33**(2), pp. 2953–2960.

[13] Zinn, B., and Lieuwen, T. C., 2005, "Combustion Instabilities In Gas Turbine Engines," *Combustion Instabilities In Gas Turbine Engines*, American Institute of Aeronautics and Astronautics, Danvers, MA, pp. 3–24.

[14] Ducruix, S., Schuller, T., Durox, D., and Candel, S., 2003, "Combustion Dynamics and Instabilities: Elementary Coupling and Driving Mechanisms," J. Propuls. power, **19**(5), pp. 722–734.

[15] Altay, H. M., Speth, R. L., Hudgins, D. E., and Ghoniem, A. F., 2009, "Flame-Vortex Interaction Driven Combustion Dynamics in a Backward-Facing Step Combustor," Combust. Flame, **156**(5), pp. 1111–1125.

[16] Palies, P., Durox, D., Schuller, T., and Candel, S., 2010, "The Combined Dynamics of Swirler and Turbulent Premixed Swirling Flames," Combust. Flame, **157**(9), pp. 1698–1717.

[17] Vogel, M., Bachfischer, M., Kaufmann, J., and Sattelmayer, T., 2021, "Experimental Investigation of Equivalence Ratio Fluctuations in a Lean Premixed Kerosene Combustor," Exp. Fluids, **62**(5), pp. 1–14.

[18] Shreekrishna, Hemchandra, S., and Lieuwen, T., 2010, "Premixed Flame Response to Equivalence Ratio Perturbations," Combust. Theory Model., **14**(5), pp. 681–714.

[19] Albrecht, P., Speck, S., Schimek, S., Bauermeister, F., Paschereit, C. O., and Gutmark, E., 2007, "Lean Blowout Control Using an Auxiliary Premixed Flame in a Swirl-Stabilized Combustor," *Collection of Technical Papers - 43rd AIAA/ASME/SAE/ASEE Joint Propulsion Conference*, Cincinatti, OH.

[20] Paschereit, C. O., and Gutmark, E., 2008, "Combustion Instability and Emission Control by Pulsating Fuel Injection," J. Turbomach., **130**(1).

[21] Seume, J. R., Vortmeyer, N., Krause, W., Hermann, J., Hantschk, C.-C., Zangl, P., Gleis, S., Vortmeyer, D., and Orthmann, A., 1998, "Application of Active Combustion Instability Control to a Heavy Duty Gas Turbine," J. Eng. Gas Turbines Power, **120**(4), pp. 721–726.

[22] Lee, J. G., Kim, K., and Santavicca, D. A., 2000, "Effect of Injection Location on the Effectiveness of an Active Control System Using Secondary Fuel Injection," Proc. Combust. Inst., **28**(1), pp. 739–746.

[23] Albrecht, P., Bade, S., Lacarelle, A., Paschereit, C. O., and Gutmark, E., 2010, "Instability Control by Premixed Pilot Flames," J. Eng. Gas Turbines Power, **132**(4), p. 041501.

[24] Dhanuka, S. K., Temme, J. E., and Driscoll, J. F., 2011, "Unsteady Aspects of Lean Premixed Prevaporized Gas Turbine Combustors: Flame-Flame Interactions," J. Propuls. Power, **27**(3), pp. 631–641.

[25] Li, J., Kwon, H., Seksinsky, D., Doleiden, D., Xuan, Y., O'Connor, J., Akiki, M., and Blust, J., 2021, "Describing the Mechanism of Instability Suppression Using a Central Pilot Flame with Coupled Experiments and

Simulations," J. Eng. Gas Turbines Power, **144**(1), p. 011015.
[26] Li, J., Peluso, S., Quay, B., Santavicca, D., Blust, J., and Nivasan, S., 2017, "Effect of Pilot Flame on Flame Macrostructure and Combustion Instability," *Proceedings of the ASME Turbo Expo*, Charlotte, NC, NC.
[27] Fu, X., Yang, F., and Guo, Z., 2015, "Combustion Instability of Pilot Flame in a Pilot Bluff Body Stabilized Combustor," Chinese J. Aeronaut., **28**(6), pp. 1606–1615.
[28] Peluso, S., Quay, B. D., Lee, J. G., and Santavicca, D. A., 2011, "Comparison Between Self-Excited and Forced Flame Response of an Industrial Lean Premixed Gas Turbine Injector," ASME 2011 Turbo Expo Turbine Tech. Conf. Expo., pp. 927–937.
[29] O'Meara, B. C., 2015, *An Experimental Study of the Effect of a Pilot Flame on Technically Pre-Mixed, Self-Excited Combustion Instabilities*, The Pennsylvania State University.
[30] Li, J., Peluso, S., and Santavicca, D., 2019, "Effect of a Premixed Pilot Flame on the Velocity-Forced Flame Response in a Lean-Premixed Swirl-Stabilized Combustor," *Proceedings of the ASME Turbo Expo*, American Society of Mechanical Engineers, Phoenix, AZ.
[31] Tyagi, A., Boxx, I., Peluso, S., and O'Connor, J., 2019, "Statistics and Topology of Local Flame–Flame Interactions in Turbulent Flames," Combust. Flame, **203**.
[32] Shanbhogue, S., Shin, D.-H., Hemchandra, S., Plaks, D., and Lieuwen, T., 2009, "Flame-Sheet Dynamics of Bluff-Body Stabilized Flames during Longitudinal Acoustic Forcing," Proc. Combust. Inst., **32**(2), pp. 1787–1794.
[33] Westfall, S., Sekulich, O., Culler, W., Peluso, S., and O'Connor, J., 2020, "Quantification of Variation in Combustion Instability Amplitude in a Multi-Nozzle Can Combustor," *ASME Turbo Expo*.
[34] Ebi, D., Doll, U., Schulz, O., Xiong, Y., and Noiray, N., 2019, "Ignition of a Sequential Combustor: Evidence of Flame Propagation in the Autoignitable Mixture," Proc. Combust. Inst., **37**(4), pp. 5013–5020.
[35] Chaudhuri, S., Kostka, S., Renfro, M. W., and Cetegen, B. M., 2010, "Blowoff Dynamics of Bluff Body Stabilized Turbulent Premixed Flames," Combust. Flame, **157**(4), pp. 790–802.
[36] Dawson, J. R., Gordon, R. L., Kariuki, J., Mastorakos, E., Masri, A. R., and Juddoo, M., 2011, "Visualization of Blow-off Events in Bluff-Body Stabilized Turbulent Premixed Flames," Proc. Combust. Inst., **33**(1), pp. 1559–1566.
[37] Coriton, B., Frank, J. H., and Gomez, A., 2013, "Effects of Strain Rate, Turbulence, Reactant Stoichiometry and Heat Losses on the Interaction of Turbulent Premixed Flames with Stoichiometric Counterflowing Combustion Products," Combust. Flame, **160**(11), pp. 2442–2456.
[38] Zhang, Q., Shanbhogue, S. J., Lieuwen, T., and O'Connor, J., 2011, "Strain Characteristics near the Flame Attachment Point in a Swirling Flow," Combust. Sci. Technol., **183**(7).
[39] Foley, C., Chterev, I., Noble, B., Seitzman, J., and Lieuwen, T., 2017, "Shear Layer Flame Stabilization Sensitivities in a Swirling Flow," Int. J. Spray Combust. Dyn., **9**(1), pp. 3–18.
[40] Hemchandra, S., Peters, N., and Lieuwen, T., 2011, "Heat Release Response of Acoustically Forced Turbulent Premixed Flames—Role of Kinematic Restoration," Proc. Combust. Inst., **33**(1), pp. 1609–1617.

